Carbon Dioxide Activation at the Ni,Fe-Cluster of Anaerobic Carbon Monoxide Dehydrogenase

Jae-Hun Jeoung, *et al.*

Science **318**, 1461 (2007);
DOI: 10.1126/science.1148481

Science (print ISSN 0036-8075; online ISSN 1095-9203) is published weekly, except the last week in December, by the American Association for the Advancement of Science, 1200 New York Avenue NW, Washington, DC 20005.

tacts are not stable or alternatively that binding occurs effectively at a single MBP site.

Next, we followed the transition from the compacted molten globulelike state to the natively folded state. Considering this transition as a single-barrier process, the probability to fold within a waiting time t is $P(t) = 1 - e^{-kt}$, where k is the folding rate. This probability can be estimated by performing multiple stretch-relaxation cycles in which the polypeptide is allowed to refold at zero load in the waiting time between the relaxation and the stretching curve. Whether folding had occurred was determined from the unfolding features during the subsequent stretching. We obtained a folding rate of $0.76 \pm 0.19\ s^{-1}$ in the absence of SecB (fig. S4). This value is similar to MBP folding rates found in bulk (*23*, *24*), which is consistent with the idea that it is the slowest folding step. We could not quantify the refolding rate in the presence of SecB because this required waiting times in the order of minutes. It is clear, however, that SecB-MBP interactions maintain MBP in the molten globulelike compacted state by perturbing the formation of stable tertiary interactions.

The single-molecule results have a direct implication for MBP translocation across the cellular membrane. Whether stable tertiary interactions are actively disrupted by the translocation machinery is a matter of debate (*17*, *27*). Our data suggest that SecB efficiently prevents any stable tertiary interactions in MBP. To test this prediction in a translocation reaction, we measured the adenosine triphosphatase (ATPase) activity during the translocation of MBP mutants with altered folding stability (*17*, *23*). We indeed found that all mutants displayed ATPase activity similar to that of wild-type preMBP (precursor form of MBP with the signal sequence) (Fig. 4C). Control experiments lacking MBP or SecB showed low ATPase activity as expected. These results support our hypothesis that for SecB-mediated translocation only limited energy is required to disrupt SecB-MBP interactions as well as tertiary intramolecular interactions in MBP. The single-molecule data provide an estimate for this energy requirement of ~$25k_BT$ (fig. S2), which roughly corresponds to the hydrolysis of one ATP molecule.

Taken together, the data indicate a folding pathway with a large variety of transitions and modes of folding (Fig. 4D), which are each affected differently by SecB: (i) The extended peptide is compacted to a molten globule state in either the presence or the absence of SecB. (ii) In the absence of SecB, folding proceeds from the molten globule to a core intermediate, but SecB prevents the formation of stable tertiary interactions, thereby maintaining the molten globulelike state. This effect may well be more general and apply also to other chaperones such as GroEL, for which there is support from other studies (*28*, *29*). (iii) Once the core intermediate has formed, SecB cannot bind, and it therefore has no effect on the folding of the external α helices onto the surface of the core structure. Folding from the core to the fully folded state exhibits similarities with a nucleation-growth mode of folding (*30*, *31*) and contrasts with the complex conformational search in the molten globulelike phase that characterizes the folding of the core. (iv) SecB also prevents the stable aggregation interactions that occur at high local MBP concentrations.

The results provide an important first step in understanding how a protein folding landscape is altered by contacts with a secondary protein. The approach is general and can be applied to interrogate other proteins and chaperone systems.

References and Notes

1. F. U. Hartl, M. Hayer-Hartl, *Science* **295**, 1852 (2002).
2. C. M. Dobson, *Nature* **426**, 884 (2003).
3. M. Rief, J. Pascual, M. Saraste, H. E. Gaub, *J. Mol. Biol.* **286**, 553 (1999).
4. R. B. Best, B. Li, A. Steward, V. Daggett, J. Clarke, *Biophys. J.* **81**, 2344 (2001).
5. A. F. Oberhauser, C. Badilla-Fernandez, M. Carrion-Vazquez, J. M. Fernandez, *J. Mol. Biol.* **319**, 433 (2002).
6. T. E. Fisher, P. E. Marszalek, J. M. Fernandez, *Nat. Struct. Biol.* **7**, 719 (2000).
7. C. Cecconi, E. A. Shank, C. Bustamante, S. Marqusee, *Science* **309**, 2057 (2005).
8. P. Fekkes, A. J. M. Driessen, *Microbiol. Mol. Biol. Rev.* **63**, 161 (1999).
9. Z. Xu, J. D. Knafels, K. Yoshino, *Nat. Struct. Biol.* **7**, 1172 (2000).
10. S. H. Lecker, A. J. M. Driessen, W. Wickner, *EMBO J.* **9**, 2309 (1990).
11. F. U. Hartl, S. Lecker, E. Schiebel, J. P. Hendrick, W. Wickner, *Cell* **63**, 269 (1990).
12. D. N. Collier, V. A. Bankaitis, J. B. Weiss, P. J. Bassford, *Cell* **53**, 273 (1988).
13. S. J. Hardy, L. L. Randall, *Science* **251**, 439 (1991).
14. N. T. M. Knoblauch *et al.*, *J. Biol. Chem.* **274**, 34219 (1999).
15. T. B. Topping, L. L. Randall, *Protein Sci.* **3**, 730 (1994).
16. L. L. Randall, T. B. Topping, S. J. Hardy, *Science* **248**, 860 (1990).
17. H. de Cock, L. L. Randall, *Mol. Microbiol.* **27**, 469 (1998).
18. B. van den Berg *et al.*, *Nature* **427**, 36 (2004).
19. A. F. Oberhauser, P. E. Marszalek, M. Carrion-Vazquez, J. M. Fernandez, *Nat. Struct. Biol.* **6**, 1025 (1999).
20. X. Duan, J. A. Hall, H. Nikaido, F. A. Quiocho, *J. Mol. Biol.* **306**, 1115 (2001).
21. Materials and methods are available on *Science* Online.
22. J. F. Marko, E. D. Siggia, *Macromolecules* **28**, 8759 (1995).
23. S. Y. Chun, S. Strobel, P. Bassford, L. L. Randall, *J. Biol. Chem.* **268**, 20855 (1993).
24. K. Beena, J. B. Udgaonkar, R. Varadarajan, *Biochemistry* **43**, 3608 (2004).
25. P. Fekkes, C. van der Does, A. J. M. Driessen, *EMBO J.* **16**, 6105 (1997).
26. J. M. Crane *et al.*, *J. Mol. Biol.* **363**, 63 (2006).
27. G. P. Liu, T. B. Topping, W. H. Cover, L. L. Randall, *J. Biol. Chem.* **263**, 14790 (1988).
28. R. Horst *et al.*, *Proc. Natl. Acad. Sci. U.S.A.* **102**, 12748 (2005).
29. G. Stan, G. H. Lorimer, D. Thirumalai, B. R. Brooks, *Proc. Natl. Acad. Sci. U.S.A.* **104**, 8803 (2007).
30. A. R. Fersht, V. Daggett, *Cell* **108**, 573 (2002).
31. A. R. Fersht, *Curr. Opin. Struct. Biol.* **7**, 3 (1997).

32. We thank P. R. ten Wolde, C. Tischer, and M. Dogterom for critical reading of the manuscript; S. Tănase-Nicola for discussions; and D. Rozeveld for technical assistance. This work was funded by the European Community Biomach program; NanoNed, a national nanotechnology program coordinated by the Dutch Ministry of Economic Affairs; and the Organization for Fundamental Research on Matter (FOM) and the Foundation for Life Sciences (ALW), which are both financially supported by the Netherlands Organization for Scientific Research (NWO). H.L.T. was supported by a VENI grant from NWO.

Supporting Online Material

www.sciencemag.org/cgi/content/full/318/5855/1458/DC1
Materials and Methods
Figs. S1 to S4
References

11 May 2007; accepted 17 October 2007
10.1126/science.1144972

Carbon Dioxide Activation at the Ni,Fe-Cluster of Anaerobic Carbon Monoxide Dehydrogenase

Jae-Hun Jeoung and Holger Dobbek*

Anaerobic CO dehydrogenases catalyze the reversible oxidation of CO to CO_2 at a complex Ni-, Fe-, and S-containing metal center called cluster C. We report crystal structures of CO dehydrogenase II from *Carboxydothermus hydrogenoformans* in three different states. In a reduced state, exogenous CO_2 supplied in solution is bound and reductively activated by cluster C. In the intermediate structure, CO_2 acts as a bridging ligand between Ni and the asymmetrically coordinated Fe, where it completes the square-planar coordination of the Ni ion. It replaces a water/hydroxo ligand bound to the Fe ion in the other two states. The structures define the mechanism of CO oxidation and CO_2 reduction at the Ni-Fe site of cluster C.

The biological redox transformations of CO_2, N_2, and H_2 are essential processes in global biogeochemical cycles and are catalyzed by enzymes containing complex metal clusters based on iron and sulfur whose detailed function is still poorly understood (*1*, *2*). Carbon monoxide dehydrogenases (CODHases) are the biological catalysts for the reversible oxidation of CO to CO_2, with water as the source of oxygen: $CO + H_2O \rightarrow CO_2 + 2e^- + 2H^+$ (Eq. 1). Two principal types of CODHases have been described that differ in their cofactor composition, structure, and stability in the presence of dioxygen: Anaerobic bacteria and archaea use oxygen-sensitive Ni- and Fe-containing CODHases, whereas aerobic, carboxydotrophic bacteria use a Cu-, Mo-, and Fe-containing flavoenzyme (*3*). The Ni,Fe-CODHases are monofunctional or bifunctional enzymes associated with Ni,Fe-containing acetyl–coenzyme A (CoA) synthases (ACS) (*4*, *5*) [for review, see (*3*, *6*)].

CO oxidation and CO_2 reduction at the active site, cluster C, of Ni,Fe-CODHases are proposed to require three different oxidation states differing by one electron (C_{red1}, C_{int}, and C_{red2}) (*6*). In this model, the C_{red1} state of cluster C converts CO to CO_2 and is formed at redox potentials below –200 mV (*7*). At pH = 7.0, the midpoint potential for the conversion of C_{red1} to C_{red2} is –530 mV (*8*, *9*), similar to the normal potential of the CO_2-CO couple of –558 mV (*10*). Consequently, C_{red2} is generated by a two-electron reduction of the C_{red1} state via C_{int} (*11*). The structure of cluster C was revealed by crystallographic analysis of CODHases isolated from *Carboxydothermus hydrogenoformans* ($CODHII_{Ch}$) and *Rhodospirillum rubrum* ($CODH_{Rr}$) at 1.6 and 2.8 Å resolution, respectively (*12*, *13*). Cluster C in $CODHII_{Ch}$ has been described as an asymmetric [$NiFe_4S_5$] center, which comprises an integral Ni ion coordinated by four sulfur ligands with square-planar geometry (*12*). An asymmetrically coordinated Fe ion (Fe1) is found close to the Ni ion. In CO-treated $CODH_{Rr}$, cluster C has a similar structure with a cubane [$NiFe_3S_4$] center linked to a mononuclear Fe site (*13*). Corresponding structures of cluster C were also identified in the crystal structures of bifunctional ACS/CODH isolated from *Moorella thermoacetica* ($CODH_{Mt}$) (*4*, *5*). Mechanisms proposed for the reversible oxidation of CO to CO_2 posit the activation of H_2O and CO as well as the stabilization of a metal-bound COO(H) intermediate. However, the structure of these states remained elusive. We describe how H_2O and CO_2 are bound and activated and propose a structure-based model for CO oxidation and CO_2 reduction at the Ni-Fe1 site of cluster C.

An expression system for $CODHII_{Ch}$ established in *Escherichia coli* enables a one-step purification of active enzyme. Crystals of recombinant $CODHII_{Ch}$ diffract up to 1.40 Å resolution on a rotating anode x-ray generator (table S1). The overall structure of recombinant $CODHII_{Ch}$ is identical to the structure of native $CODHII_{Ch}$ (*12*). $CODHII_{Ch}$ crystals were held at a defined redox potential of –600 mV for 3 hours with use of Ti(III) citrate. These crystals were either directly frozen in liquid nitrogen, generating the –600 mV state; oxidized via incubation with methylviologen (MV_{ox}) and dithiothreitol (DTT) and then incubated with DTT to give the –320 mV state; or incubated in the –600 mV solution with $NaHCO_3$ as the CO_2 source, generating the –600 mV+CO_2 state. The –600 mV state (equivalent in its redox potential to the C_{red2} state) and the –320 mV state (equivalent to the C_{red1} state) display practically identical structures for cluster C (Fig. 1, A and C). In both structures, the Ni ion is coordinated by three sulfur ligands with distorted T-shaped coordination geometry (Fig. 1, A and C, and table S3). Fe1 is coordinated by His^{261} (H261), Cys^{295} (C295), a μ_3-sulfido ligand, and a monoatomic ligand (Fig. 1, A and C, and figs. S2 and S4). A weakly occupied alternative position for Fe1 (Fe1B) is observed in both states (Fig. 1 and table S2). The monoatomic ligand is a distance of 2.7 Å from the Ni ion and occupies the position that would complete the square-planar coordination of the Ni. The electron density of the ligand can be modeled as a light atom (C, N, or O) with occupancies of about 60 to 70% or a sulfur atom with 30% occupancy. The observed Fe-ligand bond lengths of 1.93 to 1.95 Å are atypical for Fe-S bonds, whereas a H_2O/OH^- ligand is consistent with the refined bond length, the relative occupancies of ligand and Fe1 (table S2), and spectroscopic investigations of the C_{red1} state. The long distance between Ni and the ligand suggests a weak Ni-OH_x interaction. A H_2O/OH^- ligand has been detected bound to a high spin Fe^{2+} ion called ferrous component II (FCII) in the C_{red1} state (*14*, *15*), so the crystal structure is consistent with Fe1 in the –320 mV state being FCII.

In the presence of appropriate reducing agents, Ni,Fe-CODHases can catalyze the reduction of CO_2 (*16*). The structure of $CODHII_{Ch}$ with CO_2 (–600 mV+CO_2 state) reveals a triatomic ligand bridging Ni and Fe1, which replaces the water/hydroxo ligand at Fe1 (Fig. 1B). Modeling the ligand as CO_2 fully satisfies the observed electron density maps, whereas modeling with one or two

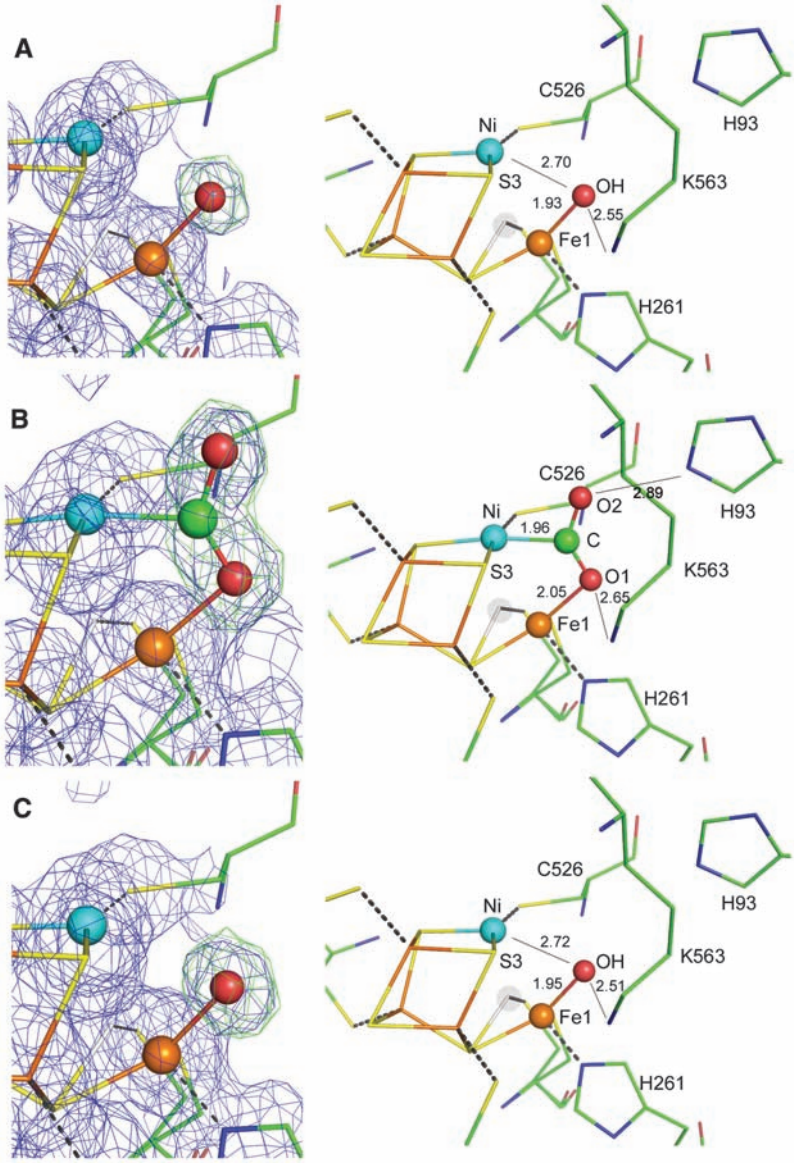

Fig. 1. The –600 mV (**A**), –600 mV+CO_2 (**B**) and –320 mV (**C**) states of cluster C. $2F_{obs} - F_{calc}$ maps in blue are contoured at 1σ, and $F_{obs} - F_{calc}$ maps in green are contoured at 4.5σ. For the calculation of the $F_{obs} - F_{calc}$ map, the OH_x ligand [(A) and (C)] and the CO_2 ligand (B) have been removed from the model. An alternative position found for Fe1, termed Fe1B, is depicted in transparent light gray. The occupancies for the alternative position have been estimated to 10 to 30%. Selected distances are shown in Å. For more details on the geometry of the three states, see figs. S2 to S4. All pictures were prepared by using PyMol (*23*).

Laboratorium Proteinkristallographie and Forschungszentrum für Bio-Makromoleküle, Universität Bayreuth, D-95440 Bayreuth, Germany.

*To whom correspondence should be addressed. E-mail: holger.dobbek@uni-bayreuth.de

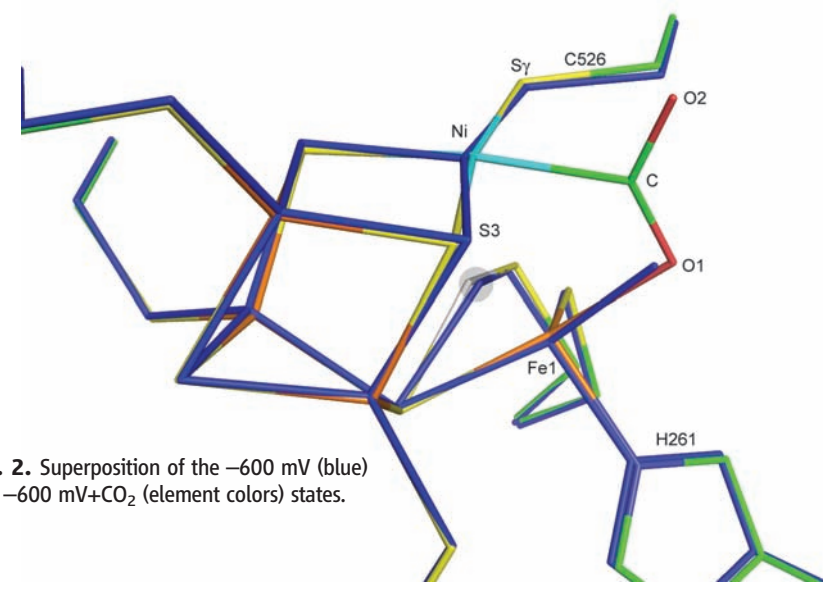

Fig. 2. Superposition of the −600 mV (blue) and −600 mV+CO_2 (element colors) states.

atoms does not. CO_2 bound to cluster C acts as a η^1 *O*CO ligand at Ni^{2+} with a Ni-C distance of 1.96 Å and completes the square-planar coordination geometry typically found for Ni^{2+} ions. CO_2 acts as a η^1 *O*CO ligand at Fe1 with an Fe1-O1 distance of 2.05 Å, resulting in a μ_2-η^2 binding mode of CO_2 bridging the Ni-Fe1 site (Fig. 1B). Like the H_2O/OH^- ligand in the –600 mV and –320 mV states, O1 of CO_2 is in hydrogen-bonding distance to Lys^{563} (K563) (Fig. 1B). O2 is in hydrogen-bonding distance to His^{93}. CO_2 binding to cluster C causes only minor changes in the geometry of the cluster (Fig. 2). The change of the distorted T-shaped to the square-planar coordination at the Ni ion induces a small shift in the Ni position of about 0.2 Å and widens the $Cys^{526}S^{\gamma}$-Ni-S_3 angle (table S3).

The ability of CO_2 to coordinate transition metal complexes is well documented (*17*). Coordination of CO_2 at the carbon atom results in a net electron transfer from the metal into the anti-

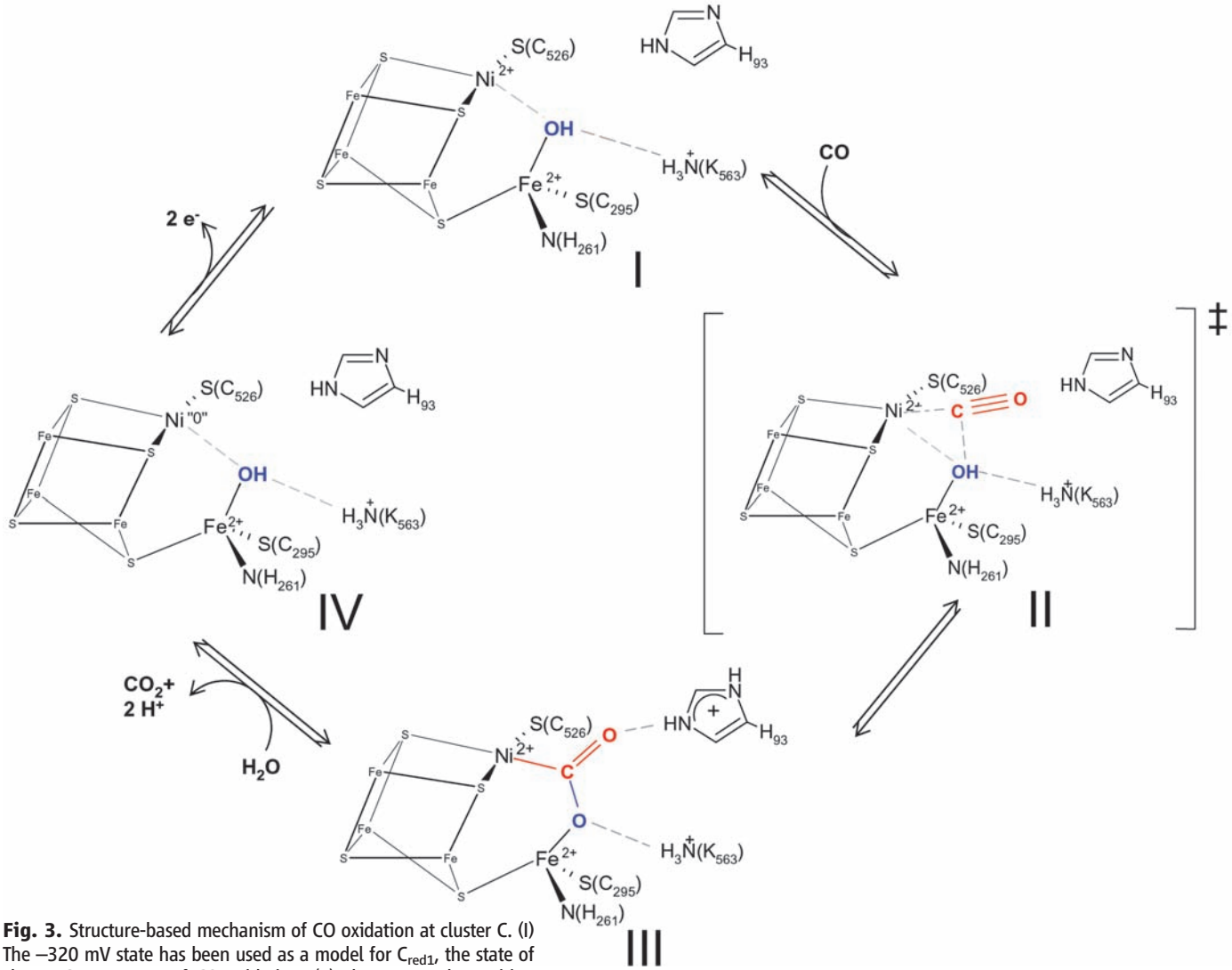

Fig. 3. Structure-based mechanism of CO oxidation at cluster C. (I) The −320 mV state has been used as a model for C_{red1}, the state of cluster C competent of CO oxidation. (II) The proposed transition state of the reaction in which CO binds to the Ni^{2+} ion and reacts with the Fe1-bound OH group. (III) The −600 mV+CO_2 state is used as a model for the stabilization of the metal carboxylate state. (IV) The −600 mV state is used as a model for the C_{red2} state, which is supposed to contain two additional electrons compared with the C_{red1} state, denoted as a formal change of the oxidation state of the Ni^{2+} ion.

bonding lowest unoccupied molecular orbital of CO_2. This activation of CO_2 increases the negative partial charges at the oxygen atoms, which are stabilized by binding to electron-deficient centers like transition metals or by forming hydrogen bonds (*17*). In the cluster C-CO_2 complex, Ni acts as the Lewis base, and Fe1 is the Lewis acid that together with K563 stabilizes the negative partial charge on O1. The deviation from linearity along the O-C-O axis [O-C-O ~133° (table S3)] is in agreement with the activation of CO_2 by binding to cluster C.

In previous structural characterizations of native preparations of CODHII$_{Ch}$, we identified a μ-sulfido ligand (S2) bridging Ni and Fe1 (*12*, *18*). The enzyme used for crystallization as well as dissolved crystals had high specific activities of ~14.000 units mg^{-1}, and on the basis of a positive correlation between the presence of the S2 ligand and enzyme activity it was postulated that S2 is essential for the catalytic CO oxidation (*18*, *19*). However, the necessity of the S2 ligand for catalysis was debated when sulfide was shown to reversibly inactivate CODH$_{Rr}$ and CODH$_{Mt}$, leading to short lag phases (*20*), and no S2 ligands were identified in the crystal structures of CODH$_{Rr}$ and CODH$_{Mt}$ (*5*, *13*). Here, we describe the structures of [NiFe$_4$S$_4$(OH$_x$)/(CO$_2$)] clusters without S2 ligand in crystals with high specific CO oxidation activities (11.000 to 13.500 units mg^{-1}), showing that the presence of S2 is not necessary for catalysis. Furthermore, the S2 ligand occupies the binding site of two substrates of Ni,Fe-CODHases, water, and CO_2. The H_2O/OH^- ligand identified requires the same coordination site at Fe1 as the bridging S2 ligand (fig. S5), and CO_2 binds to the two open coordination sites of Ni and Fe1. Thus, we suggest that the S2 ligand between Ni and Fe1 is absent in catalytically competent enzyme species and can be reductively or chemically replaced, activating the enzyme.

The three presented structures offer direct insight into the reaction mechanism (Fig. 3). The [NiFe$_4$S$_4$OH$_x$] cluster determined in the –320 mV state is the functional state that activates CO and contains the H_2O/OH^- ligand. The Ni^{2+} ion is positioned at the end of the substrate channel, and its three sulfido ligands act as π donors to the metal, enabling CO to bind to the Ni^{2+} ion (*21*). The Ni^{2+} ion has two open coordination sites, allowing either an apical binding of CO to form a distorted tetrahedral geometry or CO binding equatorially to complete the square-planar coordination geometry. Binding of CO in the apical position has been proposed for CO-treated crystals of CODH$_{Rr}$ and CODH$_{Mt}$ (*5*, *13*). Modeling of CO in the apical position places the CO-carbon atom more than 3.5 Å apart from the H_2O/OH^- ligand and makes further rearrangements necessary for the reaction to proceed. In contrast, CO binding to complete a distorted square-planar coordination of the Ni^{2+} ion results in a O*C*-*O*H$_x$ distance of less than 2 Å (Fig. 3, step II). The binding of CO to a weakly backdonating metal like Ni^{2+} results in an electrophilic carbon atom and facilitates its reaction with the Fe1-bound H_2O/OH^- ligand to a metal-carboxylate species as observed in the –600 mV+CO_2 state (Figs. 1B and 3, step III). Product release may be assisted by the reversible ligand exchange of CO_2 against H_2O at Fe1 and is accompanied by a two-electron reduction of cluster C, generating the C$_{red2}$ state. The H_2O/OH^- ligand can be replenished by a neighboring network of solvent molecules (fig. S6). A comparison of the [NiFe$_4$S$_4$OH$_x$] and [NiFe$_4$S$_4$(CO$_2$)] states reveals the positions of Ni and Fe1 to be largely unaffected by the presence or absence of the CO_2 ligand (Fig. 2). The [Fe$_3$S$_4$] site of cluster C provides a solid metal-sulfur frame in which Ni and Fe1 are held in place and serves as an electronic buffer to compensate for the electronic changes at Ni and Fe1 during the catalytic cycle. The small structural changes of cluster C agree well with the low reorganization energy expected for a reaction with turnover rates of 31,000 s^{-1} and a ratio of k_{cat} (catalytic rate constant) / K_m (Michaelis constant) of 1.7×10^9 M^{-1} s^{-1} at +70°C (*22*).

The structure-based mechanism outlined agrees in all central aspects with the bimetallic mechanism proposed on the basis of electron paramagnetic resonance (EPR), electron nuclear double-resonance (ENDOR), and Mössbauer spectroscopy (*14*, *15*).

References and Notes

1. D. C. Rees, *Annu. Rev. Biochem.* **71**, 221 (2002).
2. D. C. Rees, J. B. Howard, *Science* **300**, 929 (2003).
3. S. W. Ragsdale, *Crit. Rev. Biochem. Mol. Biol.* **39**, 165 (2004).
4. T. I. Doukov, T. M. Iverson, J. Seravalli, S. W. Ragsdale, C. L. Drennan, *Science* **298**, 567 (2002).
5. C. Darnault *et al.*, *Nat. Struct. Biol.* **10**, 271 (2003).
6. P. A. Lindahl, *Biochemistry* **41**, 2097 (2002).
7. J. Feng, P. A. Lindahl, *Biochemistry* **43**, 1552 (2004).
8. P. A. Lindahl, E. Munck, S. W. Ragsdale, *J. Biol. Chem.* **265**, 3873 (1990).
9. P. A. Lindahl, S. W. Ragsdale, E. Munck, *J. Biol. Chem.* **265**, 3880 (1990).
10. D. A. Grahame, E. DeMoll, *Biochemistry* **34**, 4617 (1995).
11. D. M. Fraser, P. A. Lindahl, *Biochemistry* **38**, 15706 (1999).
12. H. Dobbek, V. Svetlitchnyi, L. Gremer, R. Huber, O. Meyer, *Science* **293**, 1281 (2001).
13. C. L. Drennan, J. Heo, M. D. Sintchak, E. Schreiter, P. W. Ludden, *Proc. Natl. Acad. Sci. U.S.A.* **98**, 11973 (2001).
14. Z. Hu *et al.*, *J. Am. Chem. Soc.* **118**, 830 (1996).
15. V. J. DeRose, J. Telser, M. E. Anderson, P. A. Lindahl, B. M. Hoffman, *J. Am. Chem. Soc.* **120**, 8767 (1998).
16. S. A. Ensign, *Biochemistry* **34**, 5372 (1995).
17. W. Leitner, *Coord. Chem. Rev.* **153**, 257 (1996).
18. H. Dobbek, V. Svetlitchnyi, J. Liss, O. Meyer, *J. Am. Chem. Soc.* **126**, 5382 (2004).
19. S. W. Ha *et al.*, *J. Biol. Chem.* **282**, 10639 (2007).
20. J. Feng, P. A. Lindahl, *J. Am. Chem. Soc.* **126**, 9094 (2004).
21. S. A. Macgregor, Z. Lu, O. Eisenstein, R. H. Crabtree, *Inorg. Chem.* **33**, 3616 (1994).
22. V. Svetlitchnyi, C. Peschel, G. Acker, O. Meyer, *J. Bacteriol.* **183**, 5134 (2001).
23. PyMol, W. L. DeLano, DeLano Scientific, San Carlos, CA.

24. We thank W. Buckel and O. Einsle for critical reading of the manuscript and acknowledge the Deutsche Forschungsgemeinschaft (DFG grant DO 785/1) and the Fonds der chemischen Industrie (FCI) for funding. V. Svetlitchnyi is acknowledged for providing *C. hydrogenoformans* Z-2901 (strain DSM 6008) for genomic DNA preparation. Coordinates and structure factors have been deposited in the Protein Data Bank (www.pdb.org) as entries 3B51 (–600 mV state), 3B52 (–600 mV+CO_2 state), and 3B53 (–320 mV state).

Supporting Online Material

www.sciencemag.org/cgi/content/full/318/5855/1461/DC1
Materials and Methods
SOM Text
Figs. S1 to S6
Tables S1 and S2
References

30 July 2007; accepted 31 October 2007
10.1126/science.1148481

Solvent Tuning of Electrochemical Potentials in the Active Sites of HiPIP Versus Ferredoxin

Abhishek Dey,[1] Francis E. Jenney Jr.,[2] Michael W. W. Adams,[2] Elena Babini,[3] Yasuhiro Takahashi,[4] Keiichi Fukuyama,[4] Keith O. Hodgson,[1,5]* Britt Hedman,[5]* Edward I. Solomon[1,5]*

A persistent puzzle in the field of biological electron transfer is the conserved iron-sulfur cluster motif in both high potential iron-sulfur protein (HiPIP) and ferredoxin (Fd) active sites. Despite this structural similarity, HiPIPs react oxidatively at physiological potentials, whereas Fds are reduced. Sulfur K-edge x-ray absorption spectroscopy uncovers the substantial influence of hydration on this variation in reactivity. Fe-S covalency is much lower in natively hydrated Fd active sites than in HiPIPs but increases upon water removal; similarly, HiPIP covalency decreases when unfolding exposes an otherwise hydrophobically shielded active site to water. Studies on model compounds and accompanying density functional theory calculations support a correlation of Fe-S covalency with ease of oxidation and therefore suggest that hydration accounts for most of the difference between Fd and HiPIP reduction potentials.

Proteins containing Fe_4S_4 clusters catalyze one-electron transfer processes and are ubiquitous in nature (*1*–*4*). These proteins have evolved into two classes that have large differences in their electrochemical potentials: high potential iron-sulfur proteins (HiPIPs) and bacterial ferredoxins (Fds) (*5*–*8*). Physiological conditions support a reduction potential window ranging from about –600 to +500 mV (*9*). Spectroscopic and electrochemical measure-